TOXICOLOGICAL SCIENCES, 162(2), 2018, 676–687

doi: 10.1093/toxsci/kfx290
Advance Access Publication Date: January 2, 2018
Research Article

Cellular and Molecular Effects of Prolonged Low-Level Sodium Arsenite Exposure on Human Hepatic HepaRG Cells

Kostiantyn Dreval,*,[1] Volodymyr Tryndyak,*,[1] Iryna Kindrat,*,† Nathan C. Twaddle,* Orish Ebere Orisakwe,*,‡ Thilak K. Mudalige,§ Frederick A. Beland,* Daniel R. Doerge,* and Igor P. Pogribny*,[2]

*Division of Biochemical Toxicology, National Center for Toxicological Research, Jefferson, Arkansas 72079; †Department of Biological and Medical Chemistry, Ivano-Frankivsk National Medical University, Ivano-Frankivsk, Ukraine; ‡Department of Experimental Pharmacology and Toxicology, University of Port-Harcourt, Rivers State, Nigeria; and §Office of Regulatory Affairs, Arkansas Regional Laboratory, U.S. Food and Drug Administration, Jefferson, Arkansas 72079

[1]These authors contributed equally to this study.
[2]To whom correspondence should be addressed at Division of Biochemical Toxicology, National Center for Toxicological Research, 3900 NCTR Rd., Office 14C – 101, Jefferson, AR 72079. Fax: (870) 543-7136; E-mail: igor.pogribny@fda.hhs.gov.

The views expressed in this article do not necessarily represent those of the U.S. Food and Drug Administration.

ABSTRACT

Inorganic arsenic is a human carcinogen associated with several types of cancers, including liver cancer. Inorganic arsenic has been postulated to target stem cells, causing their oncogenic transformation. This is proposed to be one of the key events in arsenic-associated carcinogenesis; however, the underlying mechanisms for this process remain largely unknown. To address this question, human hepatic HepaRG cells, at progenitor and differentiated states, were continuously treated with a noncytotoxic concentration of 1 μM sodium arsenite ($NaAsO_2$). The HepaRG cells demonstrated active intracellular arsenite metabolism that shared important characteristic with primary human hepatocytes. Treatment of proliferating progenitor-like HepaRG cells with $NaAsO_2$ inhibited their differentiation into mature hepatocyte-like cells, up-regulated genes involved in cell growth, proliferation, and survival, and down-regulated genes involved in cell death. In contrast, treatment of differentiated hepatocyte-like HepaRG cells with $NaAsO_2$ resulted in enhanced cell death of mature hepatocyte-like cells, overexpression of cell death-related genes, and down-regulation of genes in the cell proliferation pathway, while biliary-like cells remained largely unaffected. Mechanistically, the cytotoxic effect of arsenic on mature hepatocyte-like HepaRG cells may be attributed to arsenic-induced dysregulation of cellular iron metabolism. The inhibitory effect of $NaAsO_2$ on the differentiation of progenitor cells, the resistance of biliary-like cells to cell death, and the enhanced cell death of functional hepatocyte-like cells resulted in stem-cell activation. These effects favored the proliferation of liver progenitor cells that can serve as a source of initiation and driving force of arsenic-mediated liver carcinogenesis.

Key words: sodium arsenite; HepaRG cells; iron metabolism; hepatocarcinogenesis.

Inorganic arsenic is a common element in the Earth's crust and an abundant environmental contaminant (Hughes *et al.*, 2011). The primary sources of human exposure to arsenic include, but are not limited to, contaminated drinking water and food (Hughes *et al.*, 2011). Chronic exposure to inorganic arsenic is associated with a broad range of noncancer and cancer

pathological states (Hughes *et al.*, 2011; IARC Monographs, 1980, 2004, 2012), and is major public health concern worldwide (Naujokas *et al.*, 2013). Inorganic arsenic was one of the earliest identified human carcinogens, the exposure to which may cause skin, lung, bladder, and liver cancers (Choiniere and Wang 2016; García-Esquinas *et al.*, 2013; IARC Monographs, 1980, 2004, 2012; Liaw *et al.*, 2008; Wang *et al.*, 2014). The carcinogenic effect of inorganic arsenic has also been demonstrated in animal studies (IARC Monographs, 2004, 2012; Tokar *et al.*, 2010a; Wanibuchi *et al.*, 2004). The most convincing evidence of arsenic carcinogenicity in animals was obtained in a "whole-life" arsenic exposure study that demonstrated the induction of a broad range of tumors, including liver cancer, in CD1 mice exposed to arsenic from fetal through adult life stages (Tokar *et al.*, 2011a; Waalkes *et al.*, 2014).

Despite strong evidence for the carcinogenicity of inorganic arsenic, the molecular mechanisms associated with arsenic carcinogenicity, including liver cancer, remained poorly understood and a subject of debate. Several mechanisms, eg, induction of oxidative stress, disruption of signaling pathways, and epigenetic alterations, have been proposed to explain arsenic carcinogenicity (Ghatak *et al.*, 2011; Meakin *et al.*, 2017; Ren *et al.*, 2010). One of the hypotheses for the tumorigenicity of arsenic focuses on its ability to target stem cells, causing the formation of a cancer-cell phenotype *in vitro* and *in vivo* (Tokar *et al.*, 2010a,b, 2011b, 2013). In particular, chronic exposure of rat kidney RIMM-18 stem/progenitor cells (Tokar *et al.*, 2013) and human prostate WPE stem cells (Tokar *et al.*, 2010b) to arsenic has been shown to induce a cancer phenotype *in vitro*. Additionally, Tokar *et al.* (2011a) showed that liver tumors in CD1 mice induced by "whole-life" arsenic exposure were highly enriched in cancer stem cells; however, the dose-response relationships and underlying mechanisms of arsenic effects on stem cells with respect to the carcinogenic process, in general, and liver carcinogenesis, in particular, remain largely unknown.

Based on these considerations, the goal of this study was to investigate cellular and molecular effects of continuous low-dose sodium arsenite ($NaAsO_2$) treatment on human hepatoma-derived nontumorigenic HepaRG cells (van Wenum *et al.*, 2017), the first human liver progenitor cell line able to differentiate into hepatocyte-like and biliary-like cells (Cerec *et al.*, 2007) and a unique model for investigating basic liver differentiation and carcinogenesis (Parent *et al.*, 2004).

MATERIALS AND METHODS

Cells and cell culture. The human progenitor hepatic HepaRG cell line was obtained from the Biopredic International (Overland Park, Kansas). The cells were maintained according to the manufacturer's recommendations. Briefly, the cells were seeded at a density of 1.3×10^4 cells/cm^2 in 100 mm dishes and maintained in William's E medium (Thermo Fisher Scientific, Waltham, Massachussets) supplemented with growth additives for HepaRG cells (Biopredic International) for 14 days. The cells were then differentiated by adding a differentiation supplement (Biopredic International) for an additional 14 days. The medium was changed every other day.

Toxicity testing. In an initial short-term cytotoxicity experiment, HepaRG cells, 28 days after seeding, were treated with 0, 0.5, 1, 5, 20, 40, 80, or 200 μM $NaAsO_2$ (Sigma-Aldrich, St Louis, Missouri). The $NaAsO_2$ was dissolved in distilled water and sterilized by filtration. After 72 h of incubation, cell viability was analyzed by a CellTiter-Glo 3D cell viability assay (Promega, Madison, Wisconsin) according to the manufacturer's protocol. The resulting dose-response curve was used to determine the IC_{10}, the concentration required to produce 10% cell death (Supplementary Figure 1). The toxicity testing assay was performed in triplicate.

In the main study, a concentration of 1 μM $NaAsO_2$ (75 ppb As), which was 3 times lower than the IC_{10}, was selected for the treatment of HepaRG cells. A concentration of 1 μM $NaAsO_2$ (75 ppb As) is well within the range of naturally contaminated groundwater drinking sources, and is substantially lower than that in drinking water in several countries in the developing world with chronic arsenic toxicity problems (eg, Bangladesh, Chile, Taiwan), where the level of As can be in the parts per million range (ppm). A concentration of 1 μM is similar to the peak levels of total arsenic species (ie, arsenite + metabolites) in livers of mice treated by gavage with 50 μg As/kg body weight (Twaddle *et al.*, 2017). Lactate dehydrogenase (LDH) release was quantified with a CytoTox-ONE Homogeneous Membrane Integrity assay (Promega) according to the manufacturer's protocol.

Treatment of HepaRG cells with $NaAsO_2$. The study design, treatment of HepaRG cells with $NaAsO_2$ and sample collection are summarized in Figure 1. Briefly, in experiment 1, 3 days after the initial seeding, 1 μM $NaAsO_2$ was added to the media. The cells were maintained in the $NaAsO_2$-containing growth media for an additional 11 days, and then in the $NaAsO_2$-containing differentiation media an additional 14 days. On the 28th day after the initial seeding, cells were harvested by mild trypsinization, washed in phosphate-buffered saline (PBS), and frozen immediately at −80°C for subsequent analyses.

In experiment 2, 14 days after the initial seeding, 1 μM $NaAsO_2$ was added to the differentiation media and the cells were maintained in the $NaAsO_2$-containing media for an additional 14 days. On the 28th day from the beginning of the study, cells were harvested by mild trypsinization, washed in PBS, and frozen immediately at −80°C for subsequent analyses.

In experiment 3, 28 days after the initial seeding, the terminally differentiated cells were treated continuously with 1 μM $NaAsO_2$ for an additional 14 days. The cells were then harvested by mild trypsinization, washed in PBS, and frozen immediately at −80°C for subsequent analyses.

Quantification of arsenic metabolites in HepaRG cells and media treated with sodium arsenite. Levels of arsenite (As^{III}) and arsenate (As^{V}), and the methylated metabolites monomethylarsonous acid (MMA^{V}) and dimethylarsinous acid (DMA^{V}) in media and HepaRG cells were determined by liquid chromatography/inductively coupled plasma-mass spectrometry (LC/ICP-MS). The levels of As^{III}, MMA^{III}, and DMA^{III} bound to thiols were determined by treating the cells with H_2O_2, which quantitatively converts trivalent arsenic to pentavalent arsenic (Naranmandura *et al.*, 2006), and subtracting the respective measurements before oxidation. Specifically, cell pellets (750 000 cells) were resuspended in 500 μl 10 mM ammonium phosphate buffer (pH 8.25) in 2.0 ml Eppendorf centrifuge tubes, and a stainless steel ball was added. The tubes were placed in a reciprocating sample disruptor (TissueLyser II, Qiagen, Hilden, Germany) and operated at 30 Hz for 3 min. The tubes were then placed in a water-filled sonicator for 10 min. After sonication, two 200 μl aliquots were taken for analysis. One aliquot was diluted with 200 μl 10 mM ammonium phosphate buffer (pH 8.25), while the other aliquot was treated with 200 μl 30% H_2O_2 at room temperature for 5 min. The solutions were then transferred to a 30k MWCO

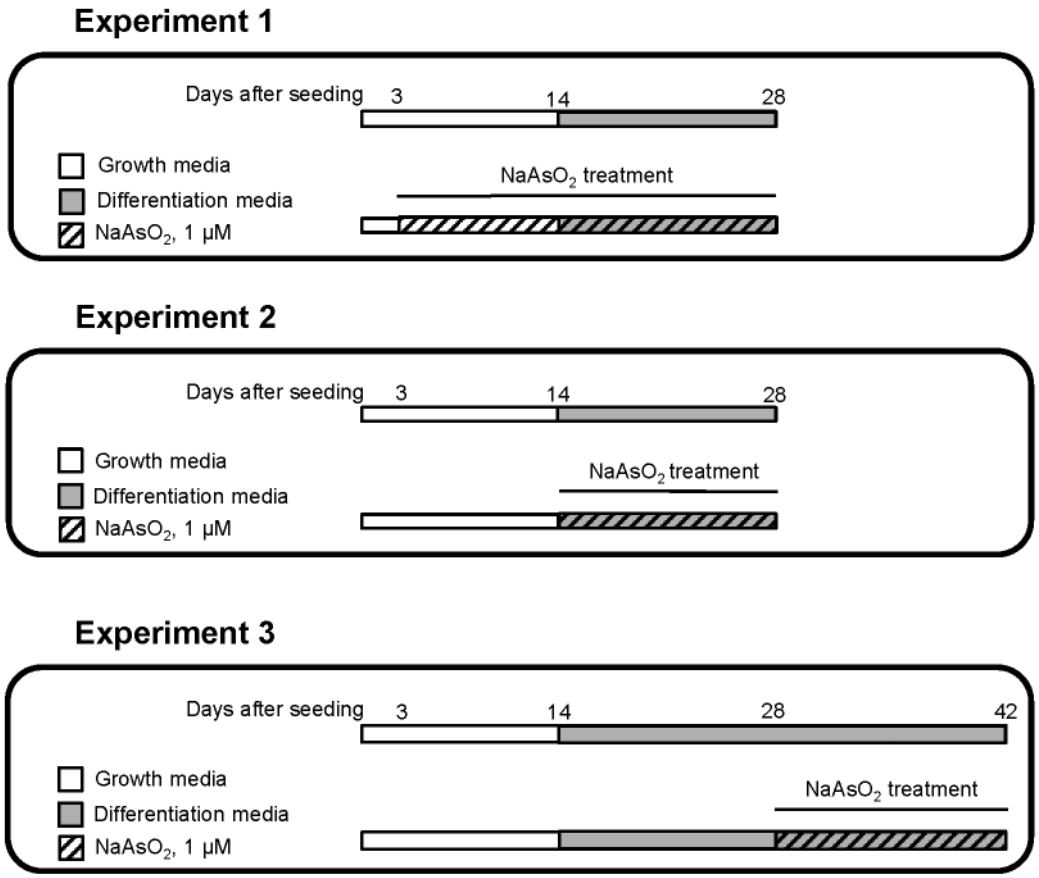

Figure 1. Diagrams of the experimental protocols. Control and $NaAsO_2$-treated HepaRG cells $NaAsO_2$ were maintained in 14 days growth media for and then for additional 14–28 days in the differentiation media. In Experiment 1: Nondifferentiated HepaRG cells, 3 days after initial seeding, were continuously treated with 1 μM $NaAsO_2$ for 25 days. The cells were collected after 28 days from initial seeding for the subsequent analyses. In Experiment 2: Nondifferentiated HepaRG cells, 14 days after the initial seeding, were treated with 1 μM $NaAsO_2$ for additional 14 days. The cells were collected after 28 days from initial seeding for the subsequent analyses. In Experiment 3: Differentiated HepaRG cells, 28 days after the initial seeding, were treated with 1 μM $NaAsO_2$ for additional 14 days and then collected for subsequent analyses. Control HepaRG cells were maintained in $NaAsO_2$-free media in all 3 Experiments.

filter (EMD Millipore, Darmstadt, Germany) and centrifuged at 14 000 × g for 15 min at 15°C. The filtrates were transferred to polypropylene vials for injection. Each sample (50 μl) was injected using an UltiMate 3000 LC system (Thermo Fisher Scientific) consisting of LC pump and autosampler. As^{III}, As^{V}, DMA^{V}, and MMA^{V} were separated with a mobile phase consisting of 98% 10 mM ammonium phosphate (pH 8.25) and 2% methanol (Thermo Fisher Scientific) at a flow rate of 1 ml/min through a Hamilton PRP-X100 LC column (4.1 × 250 mm i.d., 10 μm particle size, Reno, Nevada) with a corresponding guard cartridge, at ambient temperature. A postcolumn addition of arsenate was introduced to the system through the use of an automated switching valve (Rheodyne/IDEX, Lake Forest, Illinois) to detect and correct for changes in instrument performance. A XSeries 2 ICP-MS (Thermo Fisher Scientific) equipped with a Peltier-cooled cyclonic spray chamber, quartz torch, platinum-tipped sample cone, and Xs-style skimmer cone was operated in the collision cell technology (CCT) mode (93% He/7% H_2 collision gas) with a kinetic energy discrimination barrier for the detection of As (*m/z* 75). The use of the collision cell and kinetic energy barrier mitigated any polyatomic interferences; however, *m/z* 77 (ArCl), 82 (Se), and 83 (Kr) were also monitored.

PlasmaLab software (Thermo Fisher Scientific) was used to collect and quantify the data. Daily performance reports were generated to ensure that mass calibration and instrument performance were optimal. Quality control samples, consisting of buffer blanks, buffer blanks with H_2O_2, and As^{III}, As^{V}, MMA^{V}, and DMA^{V} standards, with and without H_2O_2, were prepared in the same manner. Injections of arsenic standards were interspersed throughout the sample runs to monitor chromatographic and detector performance. Quantification of As^{III}, As^{V}, MMA^{V}, and DMA^{V} was achieved by comparison to an external standard calibration curve prepared in 10 mM ammonium phosphate (pH 8.25) over a concentration range of 0–10 pg/μl. Typically, 3–5 concentrations were evaluated and correlation coefficients of > 0.999 were achieved. Standards of the individual arsenic species were adjusted to maintain a constant concentration of As, which was the basis for quantification.

Total RNA isolation and analysis of gene expression using microarray technology. Total RNA from control and $NaAsO_2$-treated cells was isolated using miRNeasy Mini kits (Qiagen) according to the manufacturer's instructions. Gene expression profiles of control cells ($n = 3$) and cells treated with $NaAsO_2$ ($n = 3$ per experiment) were determined using Agilent whole genome 8x60K human microarrays (Agilent Technologies, Santa Clara, California). Sample labeling and microarray processing were performed as detailed in the "One-Color Microarray-Based Gene Expression Analysis" Version 5.5 (Agilent Technologies) protocol. The hybridized slides were scanned with an Agilent DNA Microarray

scanner (Agilent Technologies) at 3 μm resolution. The resulting images were analyzed by determining the Cy3 fluorescence intensity of all gene spots (features) on each array using Agilent Feature Extraction Software (Version 11.5.1.1). The raw data were then uploaded into the ArrayTrack database (Fang *et al.*, 2009). The median fluorescence intensity of all pixels within one feature was taken as the intensity value for that feature. The raw intensity values were then normalized using 75 percentile channel scaling normalization within ArrayTrack. The lists of differentially expressed genes were generated using Benjamini-Hochberg adjusted *p*-values (Benjamini and Hochberg, 1995) to control the false discovery rate, with an adjusted *p*-value cut-off of .05, and a fold-change threshold of 1.5. The microarray gene expression data were deposited in the NCBI's Gene Expression Omnibus database (accession number GSE103873).

Functional analysis of differentially expressed genes. Ingenuity Pathway Analysis (IPA, version 33559992; Ingenuity Systems, Redwood City, California) was used to identify predicted (Z-score) clusters of biological functions across each experiment and to determine molecular network interaction among the differentially expressed genes with biological functions in each experiment.

Quantitative reverse transcription-PCR. The expression of the cytochrome P450 family 3 subfamily A member 4 (*CYP3A4*; assay ID Hs00604506_m1), transferrin (*TF*; assay ID Hs01067777_m1), transferrin receptor (*TFRC*; assay ID Hs00951083_m1), ferritin light chain (*FTL*; assay ID Hs00830226_gH), ferritin heavy chain 1 (*FTH1*; assay ID Hs01694011_s1), solute carrier family 40 member 1 (*FPN1*; assay ID Hs00205888_m1), prominin 1 (*CD133*; assay ID Hs01009250_m1), and miR-122 (assay ID 002245) was determined by quantitative reverse-transcription PCR (qRT-PCR) using the TaqMan gene expression assays (Life Technologies, Grand Island, New York). Each plate contained TaqMan gene expression assays for the experimental genes and a housekeeping β-actin (*ACTB*; assay Hs99999903_m1) gene or noncoding RNA RNU48 (assay ID 001006) as endogenous controls. The relative amount of each mRNA transcript and miR-122 was determined using the $2^{-\Delta\Delta Ct}$ method (Schmittgen and Livak, 2008).

Western blotting. Whole cell lysates containing equal quantities of proteins were separated by SDS-PAGE on 8% polyacrylamide gels and transferred to PVDF membranes. Membranes were probed with primary antibodies against caspase 3 (1:1000, Abcam, Cambridge, Massachusetts), caspase 8 (1:1000, Abcam), beclin 1 (BECN1; 1:1000, Cell Signalling Technology, Danvers, Massachusetts), LC3B (1:1000, Cell Signalling Technology), transferrin (TF; 1:500; Santa Cruz Biotechnology, Santa Cruz, California), and SRY (sex determining region Y)-box 9 (SOX9; 1:1000; Abcam). IRDye 800 conjugated secondary antigoat, antirabbit, and antimouse antibodies (1:15 000; LI-COR Biosciences, Lincoln, Nebraska) were used for visualization. Fluorescence was measured using the Odyssey CLx Infrared Imaging System (LI-COR Biosciences). IRDye 800 conjugated secondary antigoat, antirabbit, and antimouse antibodies (1:15 000; LI-COR Biosciences) were used for visualization. Fluorescence was measured using the Odyssey CLx Infrared Imaging System (LI-COR Biosciences). The images were quantified using ImageStudio 4.0 Software (LI-COR Biosciences). Equal protein loading was confirmed by immunostaining β-actin (ACTB; 1:1000; Sigma-Aldrich).

Analysis of iron content by ICP-MS. ICP-MS was used to measure the total iron content in control and $NaAsO_2$-treated cells. Microwave digestion of the cells (6×10^6) was accomplished with 4.0 ml of concentrated nitric acid (HNO_3) by the application of up to 1600 W power, 200°C for 35 min, utilizing a Microwave-Accelerated Reaction System Model MARS-X (CEM Corporation, Matthews, North Carolina), followed by quantitative transfer and dilution using 2% HNO_3. The iron content was determined with an Agilent 8800 Inductively Coupled Plasma mass spectrometer, utilizing the ^{56}Fe isotope. ^{45}Sc, at 100 ng/ml, was used as an internal standard. Helium collision cell gas was used to eliminate argon oxide ($^{40}Ar^{16}O^+$), a polyatomic interference.

Immunocytochemical detection of HMOX1 protein. Terminally differentiated HepaRG cells (on the 28th day after initial seeding) or progenitor-like HepaRG cells (on the 14th day after initial seeding) were grown on glass coverslips and treated with 1 μM $NaAsO_2$ for 24 h. After treatment, the cells were fixed with 4% neutral buffered formalin for 15 min, permeabilized in 96% ethanol/4% acetic acid solution, and blocked with 0.5% casein before the application of primary mouse monoclonal antiheme-oxygenase 1 antibody (HMOX1; dilution 1:100; Invitrogen, Rockford, Illinois) for 1 h at room temperature. The cells were washed 3 times with PBS and then incubated with secondary donkey antimouse IgG (H + L) antibodies (1:400) conjugated with Alexa Fluor 594 (Life Technologies) for 30 min at room temperature in the dark. Nuclei were counterstained with 4′, 6-diamidino-2-phenylindole dihydrochloride (Life Technologies). Phase-contrast and immunofluorescent images of the HepaRG cells were obtained and analyzed using a Leica DMi8 fluorescence microscope (Leica Microsystems Inc, Buffalo Grove, Illinois) and Leica Application Suite X (LAS X) software.

Statistical analyses. Results are presented as mean ± SD. Data were analyzed by 1-way analysis of variance, with pairwise comparisons conducted by the Student-Newman-Keuls method. Values of $p \leq .05$ were considered significant.

RESULTS

Metabolism and Disposition of $NaAsO_2$ in HepaRG Cells

LC/ICP-MS analyses were conducted to determine the ability of HepaRG cells to metabolize $NaAsO_2$. The distribution and amount of metabolites in the cell pellets were similar in all of the Experiments (Figs. 2C, 3B, and 4D). In each case, the major unbound species was arsenite (As^{III}), followed by DMA^V and then MMA^V. Arsenite represented the largest bound form within the cells also. Slightly lower binding was observed with MMA, while the binding of DMA was 4-5-fold lower. The distribution and concentration of arsenic species was also assessed in the media from Experiments 1 and 2. The major unbound species was As^{III} (841–929 nM), followed by MMA^V (47–94 nM), DMA^V (19–52 nM), and then As^V (14–16 nM). The major bound form of arsenic in the media was MMA (23–43 nM), followed by DMA (12–22 nM). Neither As^{III}, As^V, nor their methylated and dimethylated metabolites were detected in control incubations, either in cells (<0.1 pmol/10^6 cells) or media (<0.9 nM). The extensive metabolism of As^{III} is in accord with the high expression of arsenic metabolism-related *AS3MT*, *GSTO1*, and *GSTO2* genes in HepaRG cells (Supplementary Figure 2).

The Effect of $NaAsO_2$ on Nondifferentiated HepaRG Cells

Progenitor HepaRG cells actively proliferate after seeding, reaching full confluence in 14 days and then, after adding differentiation media, the cells enter a differentiation program.

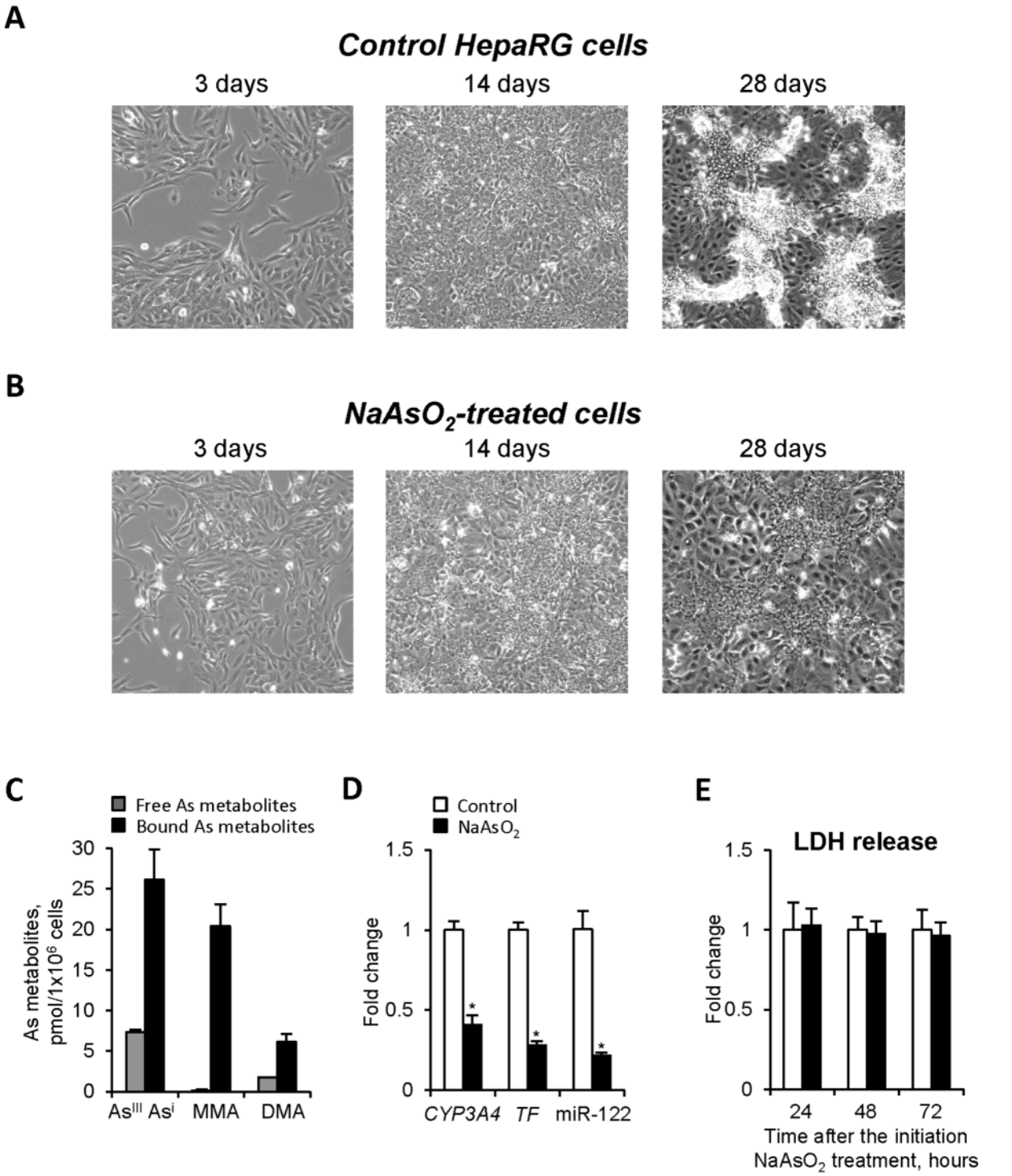

Figure 2. The effects of $NaAsO_2$ treatment on nondifferentiated human liver HepaRG cells (Experiment 1). A, Phase-contrast photographs of control HepaRG cells on the 3rd, 14th, and 28th day after the initial seeding. Original magnification ×100. B, Phase-contrast photographs of $NaAsO_2$-treated HepaRG cells on the 3rd, 14th, and 28th day after the initial seeding. Original magnification ×100. C, The concentration of arsenic species in HepaRG cells treated with $NaAsO_2$ as determined by LC/ICP-MS (see "Materials and Methods" for details). The measurements were made at the end of the treatment period. D, Expression of hepatocyte marker genes. The expression levels of *CYP3A4*, *TF*, and miR-122 is presented as a fold change in the HepaRG cells treated with $NaAsO_2$ relative to that in control HepaRG cells, which were assigned a value 1. E, Levels of LDH in the culture media 24, 48, and 72 h after the initiation of $NaAsO_2$ treatment. Values are mean ± SD, $n = 3$. Asterisks (*) denotes statistically significant ($p < .05$) difference from control HepaRG cells.

Twenty-eight days after the initial seeding, the HepaRG cells represent a mixed population of functional hepatocyte-like cells and progenitor/primitive biliary-like cells (Figure 2A). Continuous treatment of nondifferentiated progenitor-like HepaRG cells with 1 μM $NaAsO_2$ from day 3 to 28 (Experiment 1) impeded the differentiation program (Figure 2B). This was

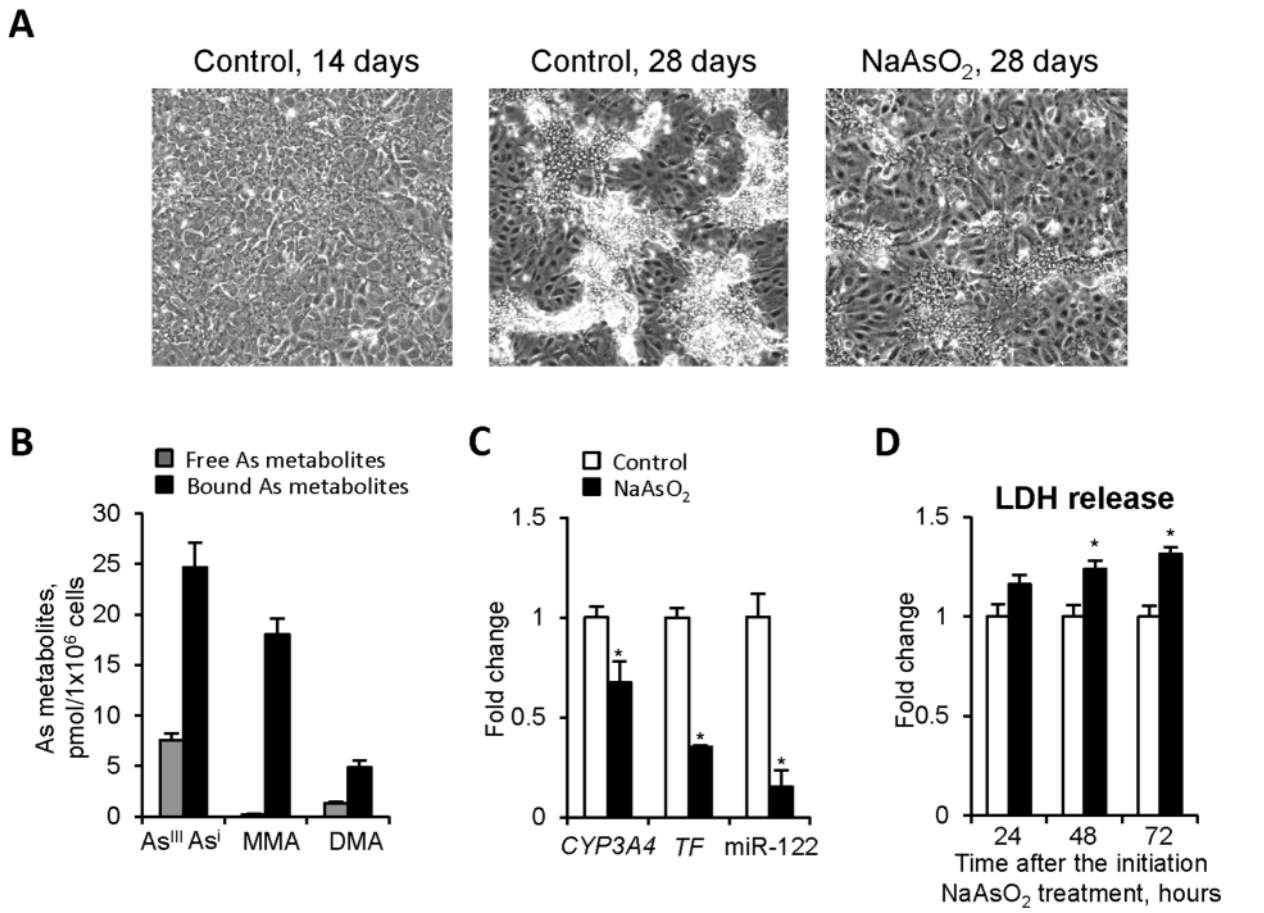

Figure 3. The effects of $NaAsO_2$ treatment on nondifferentiated human liver HepaRG cells (Experiment 2). A, Phase-contrast photographs of control HepaRG cells on the 14th and 28th day after the initial seeding and $NaAsO_2$-treated cells on the 28th day after the initial seeding. Original magnification ×100. B, The concentration of arsenic species in HepaRG cells treated with $NaAsO_2$ as determined by LC/ICP-MS (see "Materials and Methods" for details). The measurements were made at the end of the treatment period. C, Expression of hepatocyte marker genes. The expression levels of *CYP3A4*, *TF*, and miR-122 is presented as a fold change in the HepaRG cells treated with $NaAsO_2$ relative to that in control HepaRG cells, which were assigned a value 1. D, Levels of LDH in the culture media 24, 48, and 72 h after the initiation of $NaAsO_2$ treatment. Values are mean ± SD, $n = 3$. Asterisks (*) denote statistically significant ($p < .05$) difference from control HepaRG cells.

evidenced by an absence of the clusters of mature hepatocyte-like cells in the $NaAsO_2$-treated cells that were observed in the untreated control HepaRG cells. These morphological alterations were confirmed by a decreased expression of *CYP3A4*, *TF*, and miR-122 (Figure 2D), which are well-established markers of functional hepatocyte (Cardinale *et al.*, 2011; Chaudhari *et al.*, 2016; Doddapaneni *et al.*, 2013). Importantly, these arsenic-induced morphological and functional alterations were not associated with arsenic cytotoxicity, as evidenced by a lack of LDH release in the culturing media (Figure 2E). Furthermore the levels of pro-apoptotic proteins caspase 3 and caspase 8, and key autophagy-related proteins LC3B and BECN1 in progenitor HepaRG cells treated with 1 μM $NaAsO_2$ for 25 days did not differ from their levels in control cells (Supplementary Figure 3).

In Experiment 2, treatment of nondifferentiated HepaRG cells with 1 μM $NaAsO_2$ for 14 days, from day 14 to 28, resulted in cellular and molecular alterations similar to those observed in Experiment 1: an inhibition of the formation of mature hepatocyte clusters (Figure 3A) and reduced expression of *CYP3A4*, *TF*, and miR-122 (Figure 3C). There was a slight but significant increase of LDH release in $NaAsO_2$-treated cells after 48 and 72 h of treatment (Figure 3D); however, the levels of caspase 3, caspase 8, LC3B, and BECN1 proteins in progenitor HepaRG cells treated with 1 μM $NaAsO_2$ for 14 days did not differ from their levels in control cells (Supplementary Figure 3).

The Effect of Sodium Arsenite on Differentiated HepaRG Cells

Terminally differentiated HepaRG cells consist of a mixture of progenitor biliary-like cells and clusters of mature functional hepatocyte-like cells (Figure 4A). Treatment of differentiated HepaRG cells with 1 μM $NaAsO_2$ for 14 days, from day 28 to 42 (Experiment 3), resulted in a marked reduction in the number and area of functional hepatocyte-like clusters (Figure 4A). These morphological alterations were accompanied by decreased levels of *CYP3A4*, *TF*, and miR-122 (Figure 4B). In contrast, in the untreated control HepaRG cells, the area of functional hepatocyte-like clusters (Figure 4A) and the expression of *CYP3A4*, *TF*, and miR-122 (Figure 4B) were increased from day 28 to day 42. Importantly, these arsenic-induced morphological and functional alterations in terminally differentiated HepaRG cells were accompanied by an increase in cell death. This was evidenced by a substantial release of LDH into the culture media (Figure 4C); however, the levels of caspase 3, caspase 8, LC3B, and BECN1 proteins in the $NaAsO_2$-treated cells did not differ from their levels in control cells (Supplementary Figure 3).

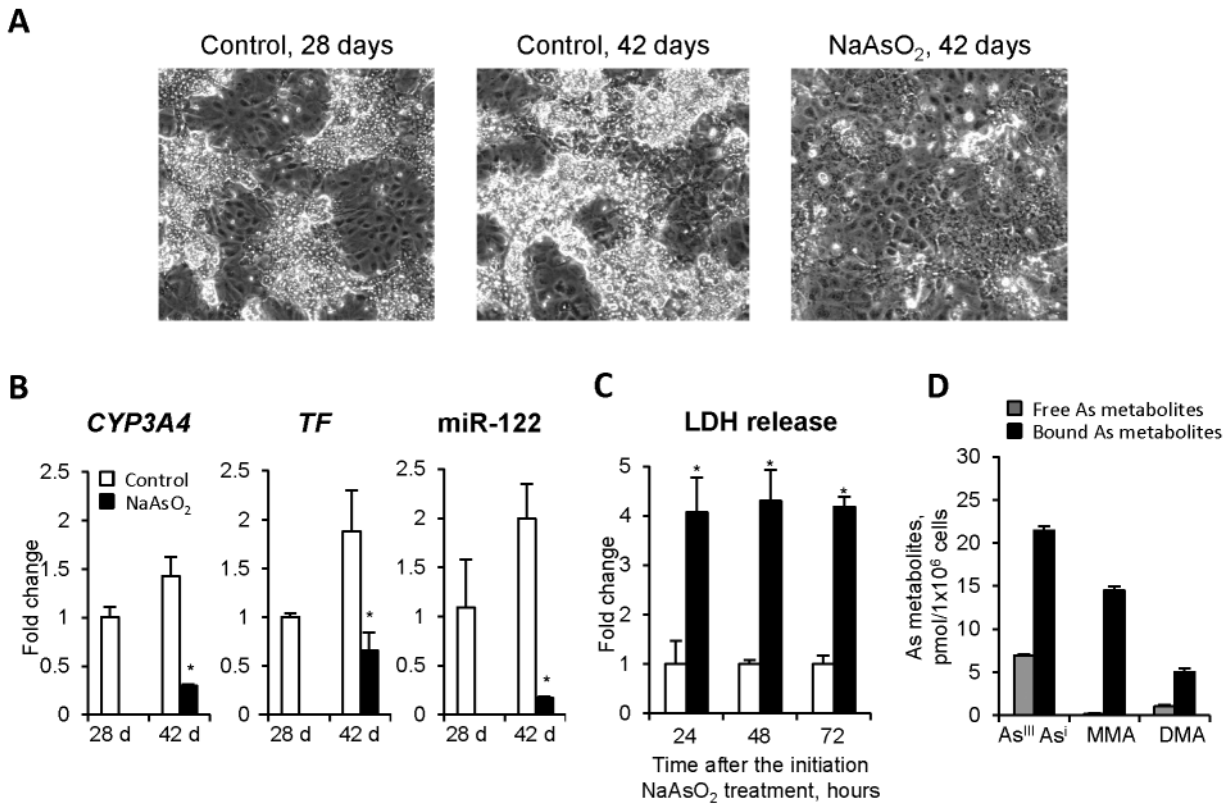

Figure 4. The effects of $NaAsO_2$ treatment on differentiated human liver HepaRG cells (Experiment 3). A, Phase-contrast photographs of control HepaRG cells on the 28th and 42nd day after the initial seeding and $NaAsO_2$-treated cells on the 42nd day after the initial seeding (14 days after $NaAsO_2$ treatment was initiated). Original magnification ×100. B, Expression of hepatocyte marker genes. The expression levels of *CYP3A4*, *TF*, and miR-122 is presented as a fold change in the HepaRG cells treated with $NaAsO_2$ relative to that in control HepaRG cells on 42 day after initial seeding, which were assigned a value 1. C, Levels of LDH in the culture media 24, 48, and 72 h after the initiation of $NaAsO_2$ treatment. Values are mean ± SD, $n = 3$. Asterisks (*) denotes statistically significant ($p < .05$) difference from control HepaRG cells. D, The concentration of arsenic species in HepaRG cells treated with $NaAsO_2$ as determined by LC/ICP-MS (see "Materials and Methods" for details). The measurements were made at the end of the treatment period.

Alteration of Gene Expression in $NaAsO_2$-Treated HepaRG Cells

To determine the underlying molecular mechanisms of $NaAsO_2$ treatment-related effects, transcriptomic profiles of control and $NaAsO_2$-treated HepaRG cells were investigated. Unsupervised hierarchical clustering of the gene expression data (Figure 5A) and principal component analysis utilizing the entire gene expression dataset (Figure 5B) showed that $NaAsO_2$-treated cells could be distinguished from their respective untreated control cells by unique transcriptomic profiles, with the patterns of gene expression in $NaAsO_2$-treated cells in Experiments 1 and 2 more closely related to each other than in Experiment 3.

Treatment of HepaRG cells with 1 μM $NaAsO_2$ resulted in profound alterations in gene expression. A total of 741, 637, and 1058 differentially expressed genes was found in $NaAsO_2$-treated cells in the Experiments 1, 2, and 3, respectively (Figure 5C, Supplementary Tables 1–3). A detailed pathway analysis of these dysregulated genes demonstrated that all $NaAsO_2$ treatment groups shared a set of common molecular pathways characterized by a strong enrichment in genes associated with cell cycle, DNA replication and repair, cell death and survival, lipid, vitamin, mineral, energy, and drug metabolism, molecular transport, and inflammatory response; however, there was a striking difference in the trends of gene expression changes in these affected pathways (Figure 5D). In particular, while lipid, vitamin, mineral, and drug metabolism, molecular transport, and energy production pathways were inhibited and the inflammatory response pathway activated in all $NaAsO_2$ treatment groups, changes in cell cycle, DNA replication and repair, cell death, survival, and proliferation, were opposite in Experiment 3 as compared with those in Experiments 1 and 2. Specifically, the cell cycle, DNA replication and repair, and cell survival and proliferation pathways were activated in nondifferentiated cells treated with $NaAsO_2$ (Experiments 1 and 2; Figure 5D). In contrast, in $NaAsO_2$-treated differentiated cells (Experiment 3), these pathways were either inhibited (cell survival and cell proliferation) or not affected (cell cycle and DNA replication and repair).

The Effect of $NaAsO_2$ Treatment on Intracellular Iron of HepaRG Cells

TF, in addition to its role as a key marker of functional hepatocytes (Chaudhari *et al.*, 2016), is also one of the main regulators of intracellular iron homeostasis (Chua *et al.*, 2007; Lane *et al.*, 2015). In light of this, the effect of $NaAsO_2$ on the status of intracellular iron homeostasis was investigated. Figure 6 shows significant alteration in the status of the intracellular iron homeostasis in HepaRG cells treated with $NaAsO_2$, characterized by altered expression of the iron metabolism-related genes, including *TFRC*, *FTL*, *FTH1*, and *FPN1* (Panels A–C). The expression changes of *TFRC*, *FTL*, and *FTH1* were similar in all $NaAsO_2$-treated groups. In contrast, the magnitude of *FPN1* overexpression, a gene that encodes the main iron exporter ferroportin, was substantially greater in $NaAsO_2$-treated nondifferentiated cells compared with differentiated cells. This resulted in an elevation of the FPN1/TFRC ratio, a condition that favors an export of intracellular iron from nondifferentiated cells, but

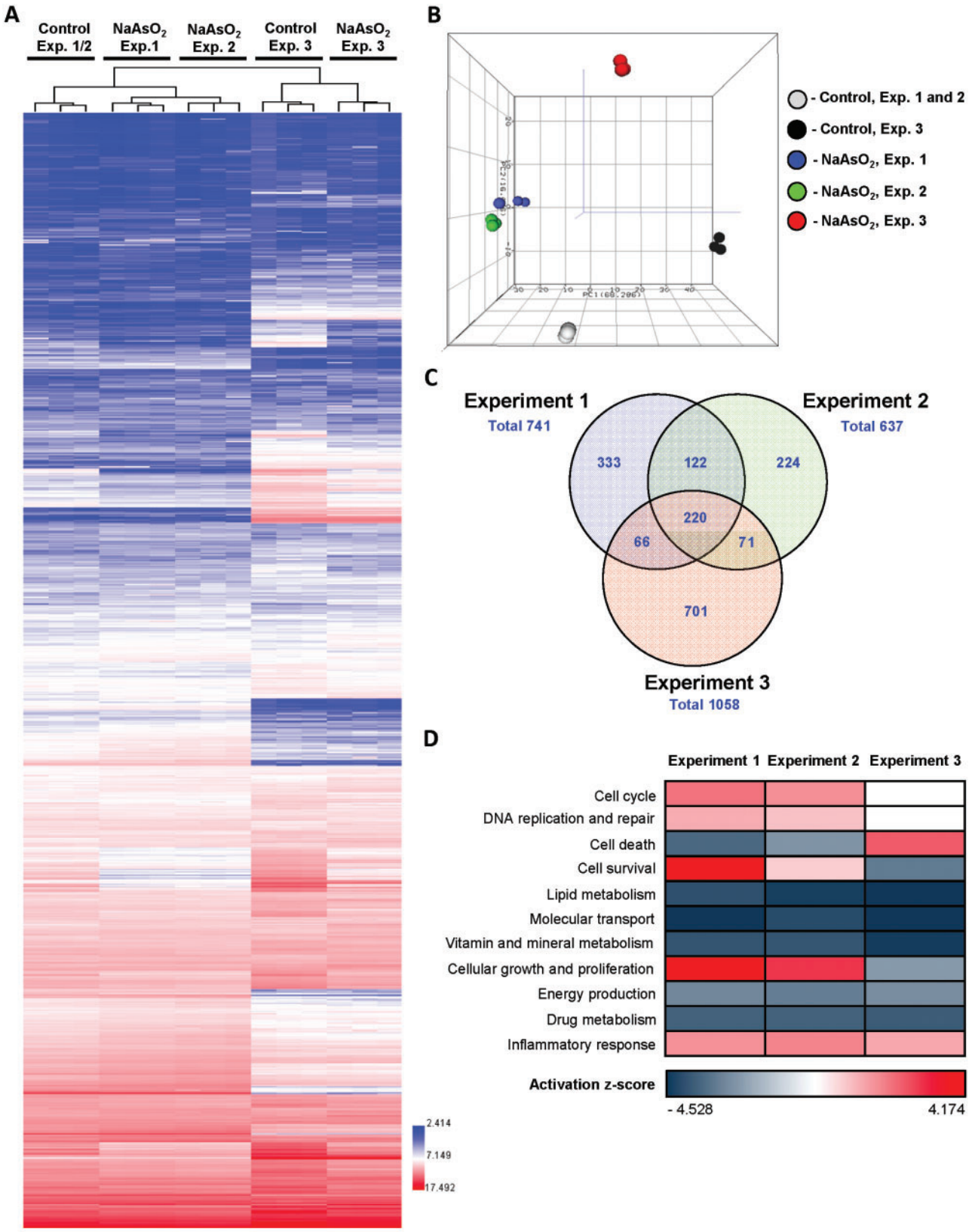

Figure 5. Whole-genome microarray transcriptomic analysis and summary of affected molecular pathways in the HepaRG cells treated with $NaAsO_2$. A, Heat maps and unsupervised hierarchical cluster analysis of log-normalized intensities illustrating differences in global gene expression profiles between control HepaRG cells and HepaRG cells treated with $NaAsO_2$ in Experiments 1–3. Color bar identifies overexpressed (red) and downregulated (blue) genes. B, Principal component analysis illustrating transcriptomic differences between control and $NaAsO_2$-treated HepaRG cells. C, Venn diagram illustrating a number of differentially expressed genes in Experiments 1–3 in $NaAsO_2$-treated HepaRG cells as compared with control cells. D, Pathway analysis of differentially expressed genes in HepaRG cells treated with $NaAsO_2$. Z-scores were calculated using IPA to predict activation (red) or inhibition (blue) of biological functions.

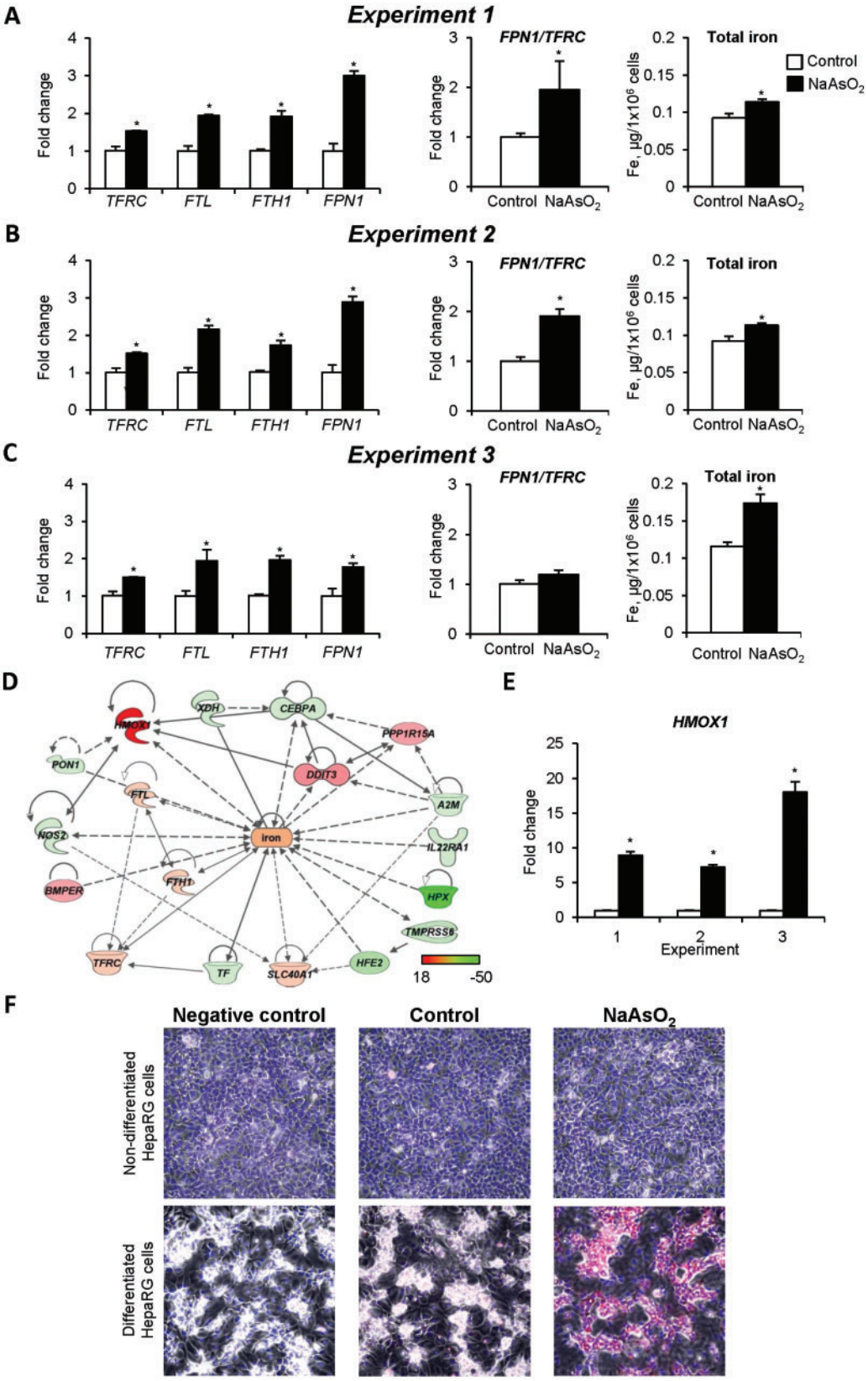

Figure 6. Dysregulation of intracellular iron homeostasis in HepaRG cells exposed to low-dose $NaAsO_2$. Expression of the iron metabolism-related genes *TFRC*, *FTL*, *FTH1*, and *FPN1*, *FPN1/TFRC* ratio, and total intracellular iron content in HepaRG cells exposed to $NaAsO_2$ in Experiment 1 (A), Experiment 2 (B), and Experiment 3 (C). D, Molecular networks of differentially expressed genes associated with the iron-metabolic molecular pathway in HepaRG cells treated with $NaAsO_2$. Red color indicates gene up-regulation and green color indicates gene down-regulation. E, Expression HMOX1 gene in HepaRG cells treated with $NaAsO_2$. The data are presented as a fold change relative to control HepaRG cells, which were assigned a value 1. F, Representative images of HMOX1 staining in nondifferentiated and differentiated control HepaRG cells and cells treated with $NaAsO_2$. The immunocytochemical analysis of the HMOX1 protein was performed as described in the "Materials and Methods" section. Positive immunostaining for HMOX1 protein is indicated by a red color. Original magnification ×200. Values are mean ± SD, $n = 3$. Asterisks (*) denote statistically significant ($p < .05$) difference from control HepaRG cells.

not from differentiated cells. Indeed, the level of intracellular iron in differentiated cells (Figure 6C) treated with arsenic was greater than in nondifferentiated cells (Figs. 6A and 6B).

The observed alterations in the status of iron metabolism in $NaAsO_2$-treated HepaRG cells were accompanied by significant changes in the expression of a number of genes associated with the iron-metabolic molecular pathway (Figure 6D). Among these genes, the overexpression of the *HMOX1* was the most prominent. In $NaAsO_2$-treated nondifferentiated HepaRG cells, the expression of *HMOX1* was 7- to 9-fold greater than control cells and this was increased to 18-fold in $NaAsO_2$-treated differentiated HepaRG cells (Figure 6E). These findings were confirmed further by immunostaining of the HMOX1 protein in $NaAsO_2$-treated HepaRG cells, which showed a marked elevation of HMOX1 protein in functional hepatocyte-like clusters (Figure 6F).

DISCUSSION

Liver cancer is one of the most aggressive and deadly human cancers (Ferlay *et al.*, 2015). Arsenic was one of the earliest identified multisite, including liver (Wang *et al.*, 2014), human carcinogens (IARC Monographs, 1980, 2004, 2012); however, there is insufficient knowledge to clarify the underlying molecular mechanisms of arsenic carcinogenicity.

This study describes some of the cellular and molecular manifestations of low-level arsenite exposure in the human HepaRG hepatic cell line at progenitor and differentiated states. The results show that the metabolism of arsenite in HepaRG cells shares many important characteristics with primary human hepatocytes (Drobná *et al.*, 2010). S-Adenosylmethionine-dependent methylation of arsenite as its triglutathione complex is predominately catalyzed by hepatic arsenite-3-methyltransferase (As3MT) (Dheeman *et al.*, 2014). The terminal product is DMA^{III}, with MMA^{III} as an intermediate that can be released from the disulfide cascade in the enzyme active site. The trivalent DMA and MMA intermediates are oxidized in the presence of molecular oxygen; and the pentavalent equivalents are the predominant species observed in hepatocyte incubations and the urine of arsenite-treated animals. In exposed humans, DMA^{V} typically exceeds MMA^{V} by approximately 10-fold in urine (U.S. Department of Health & Human Services, Centers for Disease Control and Prevention, National Center for Environmental Health, 2017). The avid binding of trivalent arsenic species with thiols is an important pathway affecting both the disposition of arsenic species and cellular biochemistry (Spuches *et al.*, 2005).

In HepaRG cells, MMA^{V} was the major metabolite observed in the cell medium and MMA^{III} was the prominent species bound intracellularly. DMA^{V} was also observed in cell media, and DMA^{III} was bound intracellularly, but in lower amounts when compared with MMA. Although the preferential production of MMA found in HepaRG cells has not been observed in hepatic microsomes or intact animals (Drobná *et al.*, 2010), it is unclear if a difference in As3MT or other factors related to dose/concentration or cofactor availability is responsible. In addition, arsenite is the predominant extracellular and intracellular species in this HepaRG experimental model. The bioactivation of As^{III} to reactive trivalent methylated species and the binding of As^{III} itself to critical thiols in catalytic, structural, and regulatory proteins are presumably the key events in toxicodynamic effects of inorganic arsenic relevant to the disease states associated with elevated arsenic intake in humans, including cardiovascular, metabolic diseases, and cancer.

One of our main findings is that exposure of HepaRG cells to $NaAsO_2$ at a low concentration, which was well within the range of naturally contaminated groundwater drinking sources, exhibited differential effects on progenitor-like cells and mature cells. It is noteworthy that this concentration of arsenite and its metabolic methylation products are likely to be within the range achievable in liver and other target tissues through consumption of naturally contaminated groundwater drinking sources. This finding was also supported by the fact that treatment of nondifferentiated HepaRG cells with 1 μM $NaAsO_2$ inhibited their differentiation into the mature hepatocyte-like cells. This process was accompanied by up-regulation of genes involved in cell growth, proliferation, and survival, while the expression of genes involved in cell death was inhibited. In contrast, treatment of differentiated hepatocyte-like HepaRG cells resulted in overexpression of cell death-related genes and down-regulation of cell proliferation genes. These changes were accompanied by a marked decrease in the levels of the functional hepatocyte markers CYP3A4, TF, and miR-122, and diminished numbers of mature functional hepatocyte-like clusters, while biliary-like cells and their markers (eg, SOX9; Supplementary Figure 4A) remained largely unaffected. Mechanistically, the cytotoxic effect of arsenic on mature hepatocyte-like HepaRG cells may be attributed, at least in part, to arsenic-induced dysregulation of cellular iron metabolism characterized by alterations favoring intracellular iron accumulation and pronounced elevation of HMOX1, an inducible form of heme oxygenase (Bauer and Bauer, 2002). In general, a moderate over-expression of HMOX1 has a cytoprotective effect; however, an excessive up-regulation of HMOX1 may sensitize cells and exhibit enhanced cytotoxicity through intracellular iron accumulation and induction of oxidative and endoplasmic reticulum stress (Rebuzzini *et al.*, 2015).

The blocking effect of $NaAsO_2$ on the differentiation of progenitor-like HepaRG cells into the mature hepatocyte-like cells was accompanied by an inhibition of cell death. These findings are in correspondence with several previous reports that showed an inhibitory effect of inorganic arsenic on differentiation of human neural (Ivanov and Hei, 2013) and kidney (Tokar *et al.*, 2013) stem cells and mouse embryonic stem cells (Rebuzzini *et al.*, 2015). The inhibitory effect of arsenic on the differentiation of progenitor-like HepaRG cells was accompanied by an apparent innate resistance to arsenic-associated cell death. A similar observation was reported by Tokar *et al.* (2013), who showed the resistance of human prostate WPE stem cells to cytolethality induced by a long-term exposure to 5 μM sodium arsenite, which was followed by an acquisition of a malignant phenotype.

The blocking effect of $NaAsO_2$ on the differentiation of progenitor cells in functional hepatocytes and the resistance of progenitor and biliary-like cells to cell death in the environment of enhanced cell death of mature hepatocyte-like resulted in a selective enrichment of cholangiocytes, which are facultative liver stem cells (Raven *et al.*, 2017). Furthermore, treatment of HepaRG cells with $NaAsO_2$, in all 3 Experiments, resulted in the over-expression of *PROM1* (*CD133*) (Supplementary Figure 4B), a critical liver cancer stem cell marker (Ma, 2013). Importantly, it has been demonstrated that, in contrast to spontaneous tumors, arsenic-induced liver tumors in mice were enriched by cancer stem cells (Tokar *et al.*, 2011a).

In summary, the findings of the present study support the hypothesis that the hepatocarcinogenic activity of inorganic arsenic can be attributed to stem-cell activation via aberrant signaling caused by binding of reactive trivalent arsenic species derived through metabolism. This hypothesis is consistent with the well-documented concept that enhanced proliferation of liver progenitor and putative adult stem cells can be a source of

initiation and a driving force in liver carcinogenesis (Marquardt *et al.*, 2015). Nevertheless, additional research is needed to determine whether or not exposure to low doses of inorganic arsenic *in vivo* will induce similar cellular alterations during primary liver carcinogenesis. The results of these studies may provide a basis for the developing of mechanism-based preventive strategies for arsenic-mediated liver cancer and arsenic-associated pathologies.

SUPPLEMENTARY DATA

Supplementary data are available at *Toxicological Sciences* online.

FUNDING

Interagency Agreement between Food and Drug Administration and National Institute of Environmental Health Sciences/National Institutes of Health (FDA IAG No. 224-12-0003/NIEHS IAG No. AES12013). This work was partly supported by the appointment of K.D. and I.K. to the Postgraduate Research Program at the NCTR administered by the Oak Ridge Institute for Science and Education (ORISE).

REFERENCES

Bauer, M., and Bauer, I. (2002). Heme oxygenase-1: Redox regulation and role in the hepatic response to oxidative stress. *Antioxid. Redox. Signal.* **4**, 749–758.

Benjamini, Y., and Hochberg, Y. (1995). Controlling the false discovery rate: A practical and powerful approach to multiple testing. *J. R. Stat. Soc. Ser. B. Stat. Methodol.* **57**, 289–300.

Cardinale, V., Wang, Y., Carpino, G., Cui, C.-B., Gatto, M., Rossi, M., Berloco, P. B., Cantafora, A., Wauthier, E., Furth, M. E., *et al.* (2011). Multipotent stem/progenitor cells in human biliary tree give rise to hepatocytes, cholangiocytes, and pancreatic islets. *Hepatology* **54**, 2159–2172.

Cerec, V., Glaise, D., Garnier, D., Morosan, S., Turlin, B., Drenou, B., Gripon, P., Kremsdorf, D., Guguen-Guillouzo, C., and Corlu, A. (2007). Transdifferentiation of hepatocyte-like cells from the human hepatoma HepaRG cell line through bipotent progenitor. *Hepatology* **45**, 957–967.

Chaudhari, P., Tian, L., Deshmukh, A., and Jang, Y.-Y. (2016). Expression kinetics of hepatic progenitor markers in cellular models of human liver development recapitulating hepatocyte and biliary cell fate commitment. *Exp. Biol. Med. (Maywood)* **241**, 1653–1662.

Choiniere, J., and Wang, L. (2016). Exposure to inorganic arsenic can lead to gut microbe perturbations and hepatocellular carcinoma. *Acta Pharm. Sin. B* **6**, 426–429.

Chua, A. C. G., Graham, R. M., Trinder, D., and Olynyk, J. K. (2007). The regulation of cellular iron metabolism. *Crit. Rev. Clin. Lab. Sci.* **44**, 413–459.

Dheeman, D. S., Packianathan, C., Pillai, J. K., and Rosen, B. P. (2014). Pathway of human AS3MT arsenic methylation. *Chem. Res. Toxicol.* **27**, 1979–1989.

Doddapaneni, R., Chawla, Y. K., Das, A., Kalra, J. K., Ghosh, S., and Chakraborti, A. (2013). Overexpression of microRNA-122 enhances in vitro hepatic differentiation of fetal liver-derived stem/progenitor cells. *J. Cell. Biochem.* **114**, 1575–1583.

Drobná, Z., Walton, F. S., Harmon, A. W., Thomas, D. J., and Stýblo, M. (2010). Interspecies differences in metabolism of arsenic by cultured primary hepatocytes. *Toxicol. Appl. Pharmacol.* **245**, 47–56.

Fang, H., Harris, S. C., Su, Z., Chen, M., Qian, F., Shi, L., Perkins, R., and Tong, W. (2009). ArrayTrack: An FDA and public genomic tool. *Methods Mol. Biol.* **563**, 379–398.

Ferlay, J., Soerjomataram, I., Dikshit, R., Eser, S., Mathers, C., Rebelo, M., Parkin, D. M., Forman, D., and Bray, F. (2015). Cancer incidence and mortality worldwide: Sources, methods and major patterns in GLOBOCAN 2012. *Int. J. Cancer* **136**, E359–E386.

García-Esquinas, E., Pollán, M., Umans, J. G., Francesconi, K. A., Goessler, W., Guallar, E., Howard, B., Farley, J., Best, L. G., and Navas-Acien, A. (2013). Arsenic exposure and cancer mortality in a US-based prospective cohort: The Strong Heart Study. *Cancer Epidemiol. Biomarkers Prev.* **22**, 1944–1953.

Ghatak, S., Biswas, A., Dhali, G. K., Chowdhury, A., Boyer, J. L., and Santra, A. (2011). Oxidative stress and hepatic stellate cell activation are key events in arsenic induced liver fibrosis in mice. *Toxicol. Appl. Pharmacol.* **251**, 59–69.

Hughes, M. F., Beck, B. D., Chen, Y., Lewis, A. S., and Thomas, D. J. (2011). Arsenic exposure and toxicology: A historical perspective. *Toxicol. Sci.* **123**, 305–332.

IARC Monographs on the Evaluation of Carcinogenic Risk of Chemicals to Humans. (1980). *Some Metals and Metallic Compounds. Vol. 23*. Lyon, France: IARC.

IARC Monographs on the Evaluation of Carcinogenic Risks to Humans. (2004). *Some Drinking-Water Disinfectants and Contaminants, Including Arsenic. Vol. 84*. Lyon, France: IARC.

IARC Monographs on the Evaluation of Carcinogenic Risks to Humans. (2012). *Arsenic, Metals, Fibres, and Dusts. Vol. 100C*. Lyon, France: IARC.

Ivanov, V. N., and Hei, T. K. (2013). Induction of apoptotic death and retardation of neuronal differentiation of human neural stem cells by sodium arsenite treatment. *Exp. Cell Res.* **319**, 875–887.

Lane, D. J. R., Merlot, A. M., Huang, M. L.-H., Bae, D.-H., Jansson, P. J., Sahni, S., Kalinowski, D. S., and Richardson, D. R. (2015). Cellular iron uptake, trafficking and metabolism: Key molecules and mechanisms and their roles in disease. *Biochim. Biophys. Acta* **1853**, 1130–1144.

Liaw, J., Marshall, G., Yuan, Y., Ferreccio, C., Steinmaus, C., and Smith, A. H. (2008). Increased childhood liver cancer mortality and arsenic in drinking water in Northern Chile. *Cancer Epidemiol. Biomarkers Prev.* **17**, 1982–1987.

Ma, S. (2013). Biology and clinical implications of $CD133^{+}$ liver cancer stem cells. *Exp. Cell Res.* **319**, 126–132.

Marquardt, J. U., Andersen, J. B., and Thorgeirsson, S. S. (2015). Functional and genetic deconstruction of the cellular origin in liver cancer. *Nat. Rev. Cancer* **15**, 653–667.

Meakin, C. J., Martin, E. M., and Fry, R. C. (2017). Epigenetic mechanisms underlying arsenic-induced toxicity. *Curr. Opin. Toxicol.* **6**, 1–9.

Naranmandura, H., Suzuki, N., and Suzuki, K. T. (2006). Trivalent arsenicals are bound to proteins during reductive methylation. *Chem. Res. Toxicol.* **19**, 1010–1018.

Naujokas, M. F., Anderson, B., Ahsan, H., Aposhian, H. V., Graziano, J. H., Thompson, C., and Suk, W. A. (2013). The broad scope of health effects from chronic arsenic exposure: Update on a worldwide public health problem. *Environ. Health Perspect.* **121**, 295–302.

Parent, R., Marion, M.-J., Furio, L., Trépo, C., and Petit, M.-A. (2004). Origin and characterization of human bipotent liver progenitor cell line. *Gastroenterology* **126**, 1147–1156.

Raven, A., Lu, W.-Y., Man, T. Y., Ferreira-Gonzalez, S., O'Duibhir, E., Dwyer, B. J., Thomson, J. P., Meehan, R. R., Bogorad, E., Koteliansky, V., *et al.* (2017). Cholangiocytes act as facultative liver stem cells during impaired hepatocyte regeneration. *Nature* **547**, 350–354.

Rebuzzini, P., Cebral, E., Fassina, L., Redi, C. A., Zuccotti, M., and Garagna, S. (2015). Arsenic trioxide alters the differentiation of mouse embryonic stem cell into cardiomyocytes. *Sci. Rep.* **5**, 14993.

Ren, X., McHale, C. M., Skibola, C. F., Smith, A. H., Smith, M. T., and Zhang, L. (2010). An emerging role for epigenetic dysregulation in arsenic toxicity and carcinogenesis. *Environ. Health Perspect.* **119**, 11–19.

Schmittgen, T. D., and Livak, K. J. (2008). Analyzing real-time PCR data by the comparative C_T method. *Nat. Protoc.* **3**, 1101–1108.

Spuches, A. M., Kruszyna, H. G., Rich, A. M., and Wilcox, D. E. (2005). Thermodynamics of the As(III)-thiol interaction: Arsenite and monomethylarsenite complexes with glutathione, dihydrolipoic acid, and other thiol ligands. *Inorg. Chem.* **44**, 2964–2972.

Tokar, E. J., Benbrahim-Tallaa, L., Ward, J. M., Lunn, R., Sams, R. L., II., and Waalkes, M. P. (2010a). Cancer in experimental animals exposed to arsenic and arsenic compounds. *Crit. Rev. Toxicol.* **40**, 912–927.

Tokar, E. J., Diwan, B. A., Ward, J. M., Delker, D. A., and Waalkes, M. P. (2011a). Carcinogenic effects of "whole-life" exposure to inorganic arsenic in CD1 mice. *Toxicol. Sci.* **119**, 73–83.

Tokar, E. J., Person, R. J., Sun, Y., Perantoni, A. O., and Waalkes, M. P. (2013). Chronic exposure of renal stem cells to inorganic arsenic induces a cancer phenotype. *Chem. Res. Toxicol.* **26**, 96–105.

Tokar, E. J., Qu, W., Liu, J., Liu, W., Webber, M. M., Phang, J. M., and Waalkes, M. P. (2010b). Arsenic-specific stem cell selection during malignant transformation. *J. Natl. Cancer Inst.* **102**, 638–649.

Tokar, E. J., Qu, W., and Waalkes, M. P. (2011b). Arsenic, stem cells, and the developmental basis of adult cancer. *Toxicol. Sci.* **120**, S192–S203.

Twaddle, N. C., Vanlandingham, M., Churchwell, M. I., and Doerge, D. R. (2017). Metabolism and disposition of arsenic species from controlled oral dosing studies with sodium arsenite in adult female CD-1 mice. I. Pilot study to determine dosing, analytical measurements, and sampling strategies. *Food Chem. Toxicol.* **111**, 482–493.

U.S. Department of Health & Human Services, Centers for Disease Control and Prevention, National Center for Environmental Health. (2017). Fourth National Report on Human Exposure to Environmental Chemicals, Updated Tables. Vol. 1, 192–227.

van Wenum, M., Treskes, P., Tang, C.-Y., Coppens, E. J., Jansen, K., Hendriks, E. J., Camus, S., van Gulik, T. M., Chamuleau, R. A. F. M., and Hoekstra, R. (2017). Scaling-up of a HepaRG progenitor cell based bioartificial liver: Optimization for clinical application and transport. *Biofabrication* **9**, 035001.

Waalkes, M. P., Qu, W., Tokar, E. J., Kissling, G. E., and Dixon, D. (2014). Lung tumors in mice induced by "whole-life" inorganic arsenic exposure at human-relevant doses. *Arch. Toxicol.* **88**, 1619–1629.

Wang, W., Cheng, S., and Zhang, D. (2014). Association of inorganic arsenic exposure with liver cancer mortality: A meta-analysis. *Environ. Res.* **135**, 120–125.

Wanibuchi, H., Salim, E. I., Kinoshita, A., Shen, J., Wei, M., Morimura, K., Yoshida, K., Kuroda, K., Endo, G., and Fukushima, S. (2004). Understanding arsenic carcinogenicity by the use of animal models. *Toxicol Appl Pharmacol.* **198**, 366–376.